Shuttling along DNA and directed processing of D-loops by RecQ helicase support quality control of homologous recombination

Gábor M. Harami[a,1], Yeonee Seol[b,1], Junghoon In[b], Veronika Ferencziová[a], Máté Martina[a], Máté Gyimesi[a], Kata Sarlós[a], Zoltán J. Kovács[a], Nikolett T. Nagy[a], Yuze Sun[b,2], Tibor Vellai[c], Keir C. Neuman[b,3], and Mihály Kovács[a,3]

[a]Department of Biochemistry, Eötvös Loránd University–Hungarian Academy of Sciences "Momentum" Motor Enzymology Research Group, Eötvös Loránd University, H-1117 Budapest, Hungary; [b]Laboratory of Single Molecule Biophysics, National Heart, Lung and Blood Institute, National Institutes of Health, Bethesda, MD 20892; and [c]Department of Genetics, Eötvös Loránd University, H-1117 Budapest, Hungary

Edited by Taekjip Ha, The Johns Hopkins University, Baltimore, MD, and approved December 7, 2016 (received for review September 15, 2016)

Cells must continuously repair inevitable DNA damage while avoiding the deleterious consequences of imprecise repair. Distinction between legitimate and illegitimate repair processes is thought to be achieved in part through differential recognition and processing of specific noncanonical DNA structures, although the mechanistic basis of discrimination remains poorly defined. Here, we show that *Escherichia coli* RecQ, a central DNA recombination and repair enzyme, exhibits differential processing of DNA substrates based on their geometry and structure. Through single-molecule and ensemble biophysical experiments, we elucidate how the conserved domain architecture of RecQ supports geometry-dependent shuttling and directed processing of recombination-intermediate [displacement loop (D-loop)] substrates. Our study shows that these activities together suppress illegitimate recombination in vivo, whereas unregulated duplex unwinding is detrimental for recombination precision. Based on these results, we propose a mechanism through which RecQ helicases achieve recombination precision and efficiency.

RecQ | helicase | magnetic tweezers | single molecule | DNA unwinding

The ability to repair DNA damage is essential for all living organisms. Homologous recombination (HR) is the most accurate DNA repair pathway, which is used to correct DNA lesions including double-strand breaks, single-strand gaps, and interstrand cross-links (1, 2). Ideally, HR occurs between allelic loci (legitimate HR), thereby avoiding genome rearrangements. However, in some cases, HR can take place between nonallelic segments containing short homologous regions, resulting in illegitimate recombination (IR). IR can lead to genome rearrangements, loss of genetic material, and altered gene functions, which ultimately lead to cell death or malignant transformation. HR must therefore be tightly controlled to preserve genome integrity. Despite their paramount importance, the mechanisms of HR quality control are largely unknown.

RecQ-family helicases are essential HR regulators in organisms ranging from bacteria to humans (1). Mutations in RecQ helicases are associated with chromosome aberrations, elevated recombination frequency, more frequent sister chromatid exchange, and cancer predisposition in higher organisms (3, 4). The capability of these helicases to unwind noncanonical DNA structures of HR intermediates is proposed to be crucial for HR progression (5, 6). In addition, RecQ helicases are thought to efficiently inhibit HR via disruption of displacement loop (D-loop) structures, early HR intermediates in which a short single-stranded DNA (ssDNA) segment invades a homologous double-stranded DNA (dsDNA) segment (7, 8). Recent studies showed that ds DNA regions are repetitively unwound and reannealed by RecQ helicases (shuttling activity), highlighting that these enzymes unwind DNA via mechanisms that are more complex than simple unidirectional strand separation (9–11). These unique shuttling and D-loop disrupting activities may serve HR quality control.

At least one RecQ homolog of each investigated organism [e.g., *Escherichia coli* RecQ, *Saccharomyces cerevisiae* Sgs1, and human Bloom's syndrome helicase (BLM)] shares a conserved modular domain architecture. It comprises two RecA-like motor domains required for ATP hydrolysis-driven ssDNA translocation with 3′–5′ directionality, a protein structure-stabilizing zinc-binding domain (ZBD) and two auxiliary DNA-binding elements: the winged-helix domain (WHD) and the helicase-and-RNaseD–C-terminal (HRDC) domain (6) (Fig. 1*A*). The WHD generally facilitates DNA unwinding and substrate recognition, and mediates protein–protein interactions (6). The HRDC domain also contributes to substrate specificity (12–14). Despite their importance in DNA processing by RecQ, the detailed mechanisms of how these accessary domains coordinate with, and modulate, RecQ activity have not been elaborated.

To elucidate the mechanistic basis of DNA processing and HR quality control by *E. coli* RecQ helicase, we used a magnetic-tweezers–based single-molecule assay to determine the contributions of the accessory domains to the unwinding activity of RecQ by measuring DNA unwinding by wild-type (WT) RecQ and RecQ variants harboring mutations in the HRDC and WHD (Fig. 1*A*). In this assay, we used two different DNA constructs to understand the effect of DNA geometry on RecQ activity: a DNA hairpin in which both ends of the DNA are under tension and a

Significance

RecQ helicase and its eukaryotic homologs are thought to play crucial roles in the quality control of homologous recombination (HR)-based DNA repair. These enzymes have multiple functions in processes that can either promote or suppress HR. A major role suggested for RecQ is the selective inhibition of illegitimate recombination events that could lead to loss of genome integrity. How can RecQ enzymes perform an exceptionally wide range of activities and selectively inhibit potentially harmful recombination events? Here, we propose a model in which the conserved domain architecture of RecQ senses and responds to the geometry of DNA substrates to achieve HR quality control.

Author contributions: G.M.H., Y. Seol, K.C.N., and M.K. designed research; G.M.H., Y. Seol, J.I., V.F., M.M., M.G., K.S., Z.J.K., and Y. Sun performed research; G.M.H., Y. Seol, J.I., V.F., M.M., M.G., K.S., N.T.N., Y. Sun, T.V., K.C.N., and M.K. analyzed data; and G.M.H., Y. Seol, V.F., K.C.N., and M.K. wrote the paper.

The authors declare no conflict of interest.

This article is a PNAS Direct Submission.

[1]G.M.H. and Y. Seol contributed equally to this work.

[2]Present address: Department of Electrical Engineering, University of Texas at Arlington, Arlington, TX 76011.

[3]To whom correspondence may be addressed. Email: mihaly.kovacs@ttk.elte.hu or neumankc@mail.nih.gov.

This article contains supporting information online at www.pnas.org/lookup/suppl/doi:10.1073/pnas.1615439114/-/DCSupplemental.

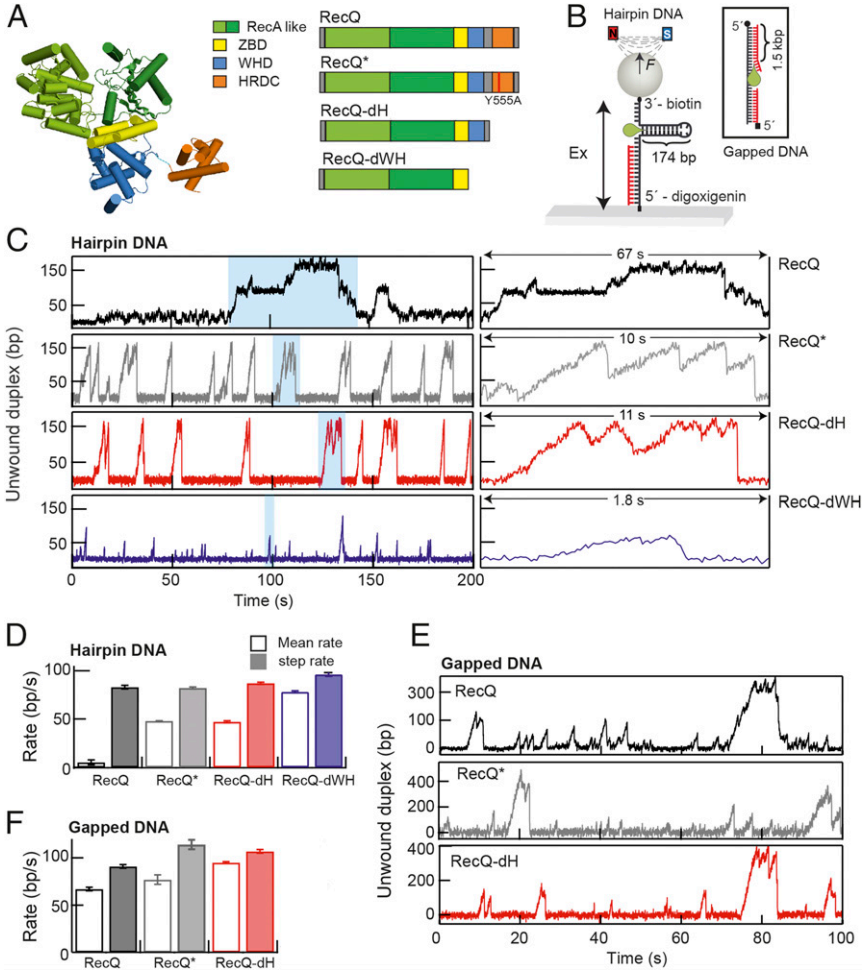

Fig. 1. The HRDC domain induces geometry-dependent pausing and shuttling during DNA hairpin unwinding. (*A*, *Left*) Structure of *E. coli* RecQ fragment comprising the core (RecA-like and ZBD domains) and the WHD [Protein Data Bank (PDB) ID code 1OYW], shown alongside that of the isolated HRDC domain (PDB ID code 1WUD). (*Right*) Domain structure of RecQ constructs used in this study. (*B*) Schematic of hairpin (main panel) and gapped (*Inset*) DNA substrates used in magnetic-tweezers experiments. The 3′-biotinylated end of the ssDNA segment of the hairpin DNA substrate was attached to a streptavidin-coated 2.8-μm magnetic bead, whereas the 5′ end of the DNA substrate was attached to a digoxigenin-labeled dsDNA handle bound to the anti-digoxigenin–coated flow cell surface. A pair of magnets pulled the bead upward, imposing a constant tension on the DNA. DNA extension (*Ex*) was measured by tracking the 3D position of the bead. The translocation direction is indicated by the green drop symbol. (*C*) Example traces of 174-bp hairpin DNA unwinding by RecQ constructs. Each trace includes multiple unwinding events typified by a gradual increase in the number of unwound base pairs followed by a rapid reannealing when the enzyme dissociated from the hairpin (*Left*). Individual unwinding events (blue shaded regions) are shown in the panels at the *Right*. The duration of each event is indicated at the *Top* of the individual plots. Fig. S1*A* includes additional hairpin DNA unwinding traces. (*D*) Mean and step rates of hairpin DNA unwinding by RecQ constructs. (*E*) Example traces of gapped DNA unwinding by RecQ, RecQ*, and RecQ-dH. Fig. S3 includes additional gapped DNA unwinding traces. (*F*) Mean and step rates of gapped DNA unwinding by RecQ constructs. Error bars in *D* and *F* correspond to the SD of Gaussian fitting parameters (Figs. S2 and S4).

gapped DNA in which only the translocating strand is under tension (Fig. 1*B*). Both DNA constructs contain a ssDNA–dsDNA junction providing a specific high-affinity binding site for a single RecQ molecule (15), which allowed us to perform the unwinding assays at low RecQ concentrations (typically, 50 pM). In addition, we developed a transient kinetic assay to monitor D-loop disruption directly. Using the engineered RecQ variants (Fig. 1*A*) permitted us to further define the mechanistic roles of the HRDC and WHD domains in disrupting D-loop HR intermediates. We show that the WHD acts as a dsDNA-binding processivity factor, whereas the HRDC domain interacts with the displaced DNA strand, inducing pausing and shuttling during unwinding of dsDNA in a hairpin, but not a gapped, geometry. Moreover, the HRDC domain orients the helicase on D-loops to promote specific disruption of the invading strand. Together, the WHD and HRDC domains enhance shuttling and D-loop processing in specific DNA geometries.

The ability to engineer the complex activities of RecQ by altering specific domains, while preserving dsDNA unwinding, enabled us to test the role of these activities in vivo. We show that shuttling and directed D-loop disruption activities mediated by the HRDC enable disruption of IR invasions, thereby supporting HR quality control. Indeed, in the absence of these complex activities, dsDNA unwinding alone is detrimental to HR precision in vivo. These results reveal that sensing of the DNA substrate geometry mediated by the HRDC and WHD domains, is a key feature enabling precise and efficient recombination by RecQ helicase.

Results

The WHD Promotes Processive Unwinding, Whereas the HRDC Domain Mediates Pausing and Shuttling. To understand how the accessory domains affect dsDNA unwinding, we generated a series of *E. coli* RecQ protein constructs (Fig. 1*A*). In addition to WT RecQ (denoted as RecQ), we generated a point mutant harboring the

Y555A substitution within the HRDC domain (denoted as RecQ*) that abolishes the HRDC–ssDNA interaction (13). We also made a HRDC deletion construct (RecQ-dH, lacking amino acid 524 onward), and a WHD-HRDC deletion construct (RecQ-dWH, lacking amino acid 415 onward) (16, 17).

We measured the unwinding activity of the constructs in a magnetic-tweezers assay using a 174-bp DNA hairpin substrate (Fig. 1*B*) at saturating ATP concentration (1 mM; Table S1). Unwinding by RecQ was typified by numerous pauses often accompanied by periods of repetitive unwinding and reannealing, collectively referred to as shuttling. Reannealing events occurred on two timescales: (*i*) slow reannealing, suggesting closure of the hairpin behind the helicase as it translocated on ssDNA after completely unwinding the hairpin; and (*ii*) rapid incomplete reannealing (abrupt reduction of DNA extension followed by a gradual increase in DNA extension), suggesting transient release or backsliding of the helicase core along ssDNA (Fig. 1*C* and Fig. S1). Rapid incomplete reannealing events spanning more than 50 bp were occasionally observed but were not considered as shuttling as they are indistinguishable from events in which RecQ dissociates from the hairpin junction and the hairpin is prevented from completely reannealing by a second RecQ bound to distal ssDNA (*SI Materials and Methods*). In contrast to the frequent pausing and shuttling by RecQ throughout the hairpin, we found that the HRDC point mutant RecQ* unwound the hairpin efficiently with substantially shorter pauses and dissociated rapidly with less frequent shuttling events once the hairpin was unwound (Fig. 1*C*, Fig. S1, and Table 1). Deletion of the HRDC domain (RecQ-dH) further reduced the pausing and shuttling frequency, suggesting that the effects of the HRDC domain are largely, but not entirely, due to ssDNA binding mediated by Tyr^{555} (Fig. 1*C*, Fig. S1, and Table 1). In particular, RecQ* exhibited shuttling behavior at the end of DNA hairpin similar to that of RecQ, consisting of pausing and short-distance unwinding followed by fast reannealing (Fig. S1*B*). On the other hand, RecQ-dH exhibited either rapid disassociation or slow reannealing and unwinding over larger extents (>50 bp) at the end of the hairpin (Fig. S1*B*). Further deletion of the WHD (RecQ-dWH) significantly decreased the processivity (number of DNA base pairs unwound during a single binding event), indicating that the WHD stabilizes RecQ on DNA during unwinding (Fig. S2).

The mean hairpin unwinding rate (i.e., between the initial and maximum unwinding positions) of RecQ was severalfold slower than that of the mutant constructs (Fig. 1*D*, Fig. S2, and Table 1). This large difference resulted from frequent, long-duration, pauses as the step rates (i.e., between pauses) for all constructs were comparable (Fig. 1*D* and Table 1). The marked reduction of the median run length of RecQ-dWH compared with the WHD-containing constructs demonstrates that the WHD significantly contributes to the processivity of unwinding (Fig. S2 and Table 1; see also below).

Helicase pausing appeared to be more frequent at certain positions on the hairpin. For example, many pauses occurred near the 100-bp unwinding position (Fig. 1 and Fig. S1). This behavior may reflect sequence-dependent unwinding and/or pause kinetics, as has been observed for other superfamily (SF) 1 and 2 helicases including hepatitis virus NS3 helicase (18), XPD helicase (19), and RecBCD helicase (20). Additional experiments will be required to characterize the sequence dependence of RecQ unwinding and pausing, and the role of the HRDC domain in these processes.

The RecQ HRDC Domain Binds to the Displaced DNA Strand During Unwinding. The above results led us to suspect that the frequent pausing by RecQ is caused by binding of the HRDC domain to one of the nascent ssDNA strands during hairpin unwinding, consistent with the ssDNA-binding capability of the isolated HRDC domain (13). As both ssDNA strands are under tension in the hairpin substrate (Fig. 1*B*), the binding of the HRDC domain to either strand could transiently stall the enzyme. To determine the ssDNA-binding geometry of HRDC-dependent pausing, we measured RecQ unwinding on a gapped dsDNA substrate (Fig. 1*B*, *Inset*). Here, unlike in the hairpin substrate, the displaced ssDNA segment (i.e., the one complementary to the tracking strand) is not under tension. Thus, if the HRDC domain bound to the displaced ssDNA, it would not hinder progression of the enzyme. On the other hand, significant pausing similar to that observed with the DNA hairpin would occur if the HRDC bound the tracking ssDNA strand or the dsDNA ahead of the enzyme. We observed no significant pauses during unwinding of the gapped DNA substrate by RecQ (Fig. 1*E* and Fig. S3). Moreover, the mean unwinding rates of RecQ, RecQ*, and RecQ-dH on the gapped DNA substrate were comparable, indicating that pausing and shuttling during unwinding of the hairpin substrate is mediated by HRDC binding to the displaced ssDNA strand (Fig. 1*F*, Fig. S4, and Table 1). Nonetheless, RecQ displays an overall less efficient helicase activity than RecQ-dH (Table 1), suggesting that the HRDC inherently regulates RecQ core unwinding activity (see below). This may be important to

Table 1. Mechanistic parameters of RecQ constructs

Construct	RecQ	RecQ*	RecQ-dH	RecQ-dWH
DNA unwinding[†]				
Mean rate, bp/s	5.0 ± 2.6 (67 ± 2)	48 ± 0.3 (77 ± 5)	47 ± 1 (95 ± 1)	78 ± 1
Step rate, bp/s	83 ± 2 (91 ± 2)	82 ± 1 (114 ± 5)	87 ± 1 (107 ± 2)	96 ± 2
Shuttling frequency, % of *N*[‡]	85 (28)	53 (17)	39 (17)	N.D.
Shuttling frequency at the end of DNA hairpin, % of *N**	85 (N.D.)	57 (N.D.)	39 (N.D.)	N.D.
Shuttling duration, s[‡]	13 ± 3 (2.4 ± 0.3)	2.0 ± 0.2 (2.4 ± 0.8)	2.3 ± 0.6 (2.8 ± 1)	N.D.
Median run length, bp	104 ± 4 (78 ± 1)	143 ± 1 (113 ± 2)	157 ± 1 (237 ± 11)	47 ± 1
Total number of complete unwinding events, *N**	20 (N.D.)	69 (N.D.)	100 (N.D.)	N.D.
Total number of unwinding events, *N*	95 (141)	76 (87)	100 (30)	193
ssDNA binding and ATP-driven translocation				
K_d, dT_{54}, nM[§]	34 ± 4	38 ± 3	91 ± 18	>3,000
Occluded site size, nt per protein monomer,[¶]	28 ± 2	27 ± 3	27 ± 2	19 ± 3
Translocative ATPase (k_{trans}), s^{-1}[#]	32 ± 1	37 ± 1	54 ± 1	47 ± 2

N.D., not determined. Additional mechanistic parameters are shown in Table S1.

[†]Magnetic-tweezers data obtained with hairpin DNA substrate (gapped DNA data in parentheses) (Fig. 1 and Figs. S1–S4). Reported errors are SDs of fits.

[‡]The reported shuttling frequency (duration) includes shuttling events occurring during unwinding and at the end of the hairpin DNA substrate, and indicates strand-switching frequency (duration) for gapped DNA in parentheses.

[§]From fluorescence anisotropy titrations (Fig. S5*A*).

[¶]From oligo-dT length dependence of the apparent DNA dissociation constant during ATPase activity (Fig. S5*C*), based on Eqs. **S1** and **S2**.

[#]From oligo-dT length dependence of ATPase k_{cat} (Fig. S5*D*), based on Eqs. **S1** and **S3**.

maintain the balance between exonuclease such as RecJ and helicase unwinding or to naturally prevent long ssDNA exposure during DNA resection at the initial DNA recombination step (21, 22).

All RecQ constructs displayed occasional strand-switching events before dissociating from the gapped DNA substrate (Table 1). This behavior is distinct from the shuttling observed with the WT enzyme on the hairpin substrate, and is clearly independent of the HRDC domain, as it was observed for all constructs.

During ssDNA Translocation, the WHD Contributes to DNA Binding, Whereas the HRDC Domain Suppresses the ATPase Activity. To further dissect the mechanistic roles of the WHD and HRDC domains, we evaluated their effects on DNA binding and DNA-activated ATP hydrolysis using ssDNA (oligo-dT) substrates. Fluorescence anisotropy titrations of 3′–Cy3-labeled dT_{54} showed that the WHD markedly, whereas the HRDC domain moderately, contributes to the ssDNA binding affinity of RecQ in the absence of ATP (Fig. S5*A* and Table 1). As previously shown (23–25), the ssDNA binding affinity and the occluded site size of helicases on ssDNA during ATP hydrolysis can be deduced from the ssDNA concentration dependence of their ATPase activity (Fig. S5*B*). We found that the occluded site size of RecQ on ssDNA (per protein monomer) is not influenced by HRDC deletion, but it is significantly reduced by WHD deletion (Fig. S5*C* and Table 1).

The DNA-free ATPase activity (k_{basal}) of RecQ was unaffected by the WHD and/or HRDC domains, indicating an intact motor core for all constructs (Table S1). However, the ssDNA-activated ATPase activity (k_{cat}) was suppressed by the HRDC domain (Fig. S6 *B* and *D*) in line with our previous report (17), without influencing the ATP binding affinity to the motor core (K_{ATP}, Table S1). Furthermore, ATPase suppression was not related to the ssDNA binding ability of the RecQ HRDC domain as RecQ and RecQ* showed similar k_{cat} values (Fig. S6 *B* and *D*, and Table 1). These results suggest that the HRDC domain of RecQ suppresses ATP hydrolysis via interactions with the motor core. Similar HRDC-dependent suppression of the ATPase activity has been shown for human BLM (26).

The WHD and HRDC Domains Enable Directed Processing of D-Loop Structures. In addition to its roles in dsDNA unwinding and ATPase modulation, the HRDC domain has been implicated in the processing of DNA substrates containing an invading DNA strand (12), for example, D-loop structures formed during recombination. To decipher the mechanism of D-loop processing and to dissect the roles of the WHD and HRDC domains in the process, we developed a kinetic assay to monitor the enzymatic processing of three related fluorescently labeled DNA substrates (Fig. 2 and Figs. S6 and S7). (*i*) We recorded the time courses of formation and disappearance of all intermediates during the unwinding of a four-stranded D-loop–like substrate (DL4) (Fig. 2, Fig. S6 *A* and *B*, and Tables S1 and S2). In separate experiments, we monitored the unwinding of (*ii*) a three-stranded D-loop-like substrate (DL3), and (*iii*) a two-stranded, 3′-tailed DNA structure (3T) (Fig. 2). (DL3 and 3T are constituents of DL4, as depicted in Fig. 2*A*.) In the unwinding experiments, RecQ constructs premixed with labeled DNA substrates (DL4, DL3, or 3T) were mixed with excess ATP and a large excess of unlabeled ssDNA trap (with a sequence identical to that of the labeled invading strand) to inhibit DNA reannealing and enzyme rebinding to labeled substrates after dissociation. We note that the DL4 preparations contained fractions of the DL3 and 3T species (Fig. 2 and Fig. S6 *A* and *B*). However, the initial heterogeneity of DL4 preparations turned out to be useful as the fraction of each DNA species could be accurately determined throughout the time courses—which, in conjunction with separate DL3 and 3T unwinding experiments, facilitated robust determination of the kinetic mechanism by global fitting analysis of all reactions (see below).

In general, the disappearance of DL4 was accompanied by a transient accumulation of 3T, which was eventually converted to ssDNA; whereas in the separately performed DL3 and 3T unwinding experiments, both substrates showed biphasic disappearance profiles (Fig. 2 *B*–*E*). The simplest kinetic model accounting for these behaviors involves multiple D-loop processing pathways dictated by different enzyme–DNA binding configurations and the 3′–5′ unwinding directionality of RecQ (Fig. 2*A*). In the model, a fraction of initial enzyme–DL4 and enzyme–DL3 complexes (DLI in Fig. 2*A*) is oriented for disruption of the invasion, producing 3T from DL4 or ssDNA from DL3, as the enzyme tracks the strand to which the invading strand is annealed. In a second fraction (DLE), the enzyme is oriented "outward" from the invasion and thus will produce DL3 from DL4—or, in the case of the DL3 substrate, leave the substrate intact. In a third fraction (DLI′), the enzyme tracks the invading strand starting from its 3′ end, thus producing ssDNA from either DL4 or DL3. In the remainder of the cases (represented by the DLN fraction), no unwinding of DL4 or DL3 occurs, either because the enzyme unwinds one of the dsDNA arms flanking the invasion (which will then rapidly reanneal), or due to premature termination of unwinding initiated from any of the possible initial binding configurations. Unwinding of the 3T substrate occurs from a single binding configuration (3TE), whereas 3TN represents the fraction of enzyme–3T complexes that are not unwound.

For parsimony, successful unwinding of any of the dsDNA segments in the DNA substrates was modeled to occur with a single rate constant k_U, as the lengths of these segments were similar (21-bp invasion, 20-bp other segments). k_U was also used as a lower bound for the rate constant of nonproductive unwinding events (represented in the DLN and 3TN fractions). After termination of a single unwinding run, slow rebinding of the enzyme to the DNA substrates (hindered but not completely inhibited by the ssDNA trap strand) was modeled to occur at rate constant k_R for DL4 and DL3, or k_R' for 3T (k_R, $k_R' << k_U$). The initial partitioning of enzyme–substrate complexes, as well as the four rate constants of the model, were determined by global kinetic fitting of the DL4, DL3, and 3T unwinding reactions of individual RecQ constructs (Fig. 2 *B*–*E* and Table S1). In the best-fit models, the DLE fraction was 0 for all assessed constructs, indicating that this pathway does not occur in RecQ reactions (Table S1). Apart from DLE, the omission of any further element of the model resulted in significant deterioration of the fits, indicating that the model comprising the DLI, DLI′, and DLN pathways represents the simplest plausible description of the reactions.

As depicted in Fig. 2*A*, the DLI and DLI′ fractions represent disruption of the invading strand in D-loop–like substrates, either starting from the branch point (DLI) or the 3′ end of the invading strand (DLI′). In vivo, analogous D-loop disruption results in termination of HR initiation. Conversely, the DLN (and DLE) fractions represent maintenance of the invading strand. As mentioned above, DLN represents the sum of short, unproductive unwinding runs (in any orientation) plus unwinding events targeted at either of the flanking dsDNA "arms" of the D-loop–like substrates (bottom left and right arms in the DL4 and DL3 structures drawn in Fig. 2*A*). All of these DLN events are followed by substrate DNA reannealing and are thus not detected in our assay (Fig. 2*A*). In the case of enzymes that are highly processive and bind D-loop–like substrates with high affinity (such as RecQ* and RecQ-dH; Fig. 1*C* and Fig. S7 *C* and *D*), short unwinding runs are rare and DLN will thus dominantly represent unwinding of dsDNA arms. Analogous unwinding events in D-loops in vivo are likely to extend and stabilize the invasion and, thus, propagate HR, either by moving the invasion branch point away from the 3′ end of the invading strand (unwinding of the bottom left dsDNA arm in Fig. 2*A*), or by liberating template for the DNA synthetic extension of the 3′ end of the invading strand (unwinding of the bottom right arm in Fig. 2*A*).

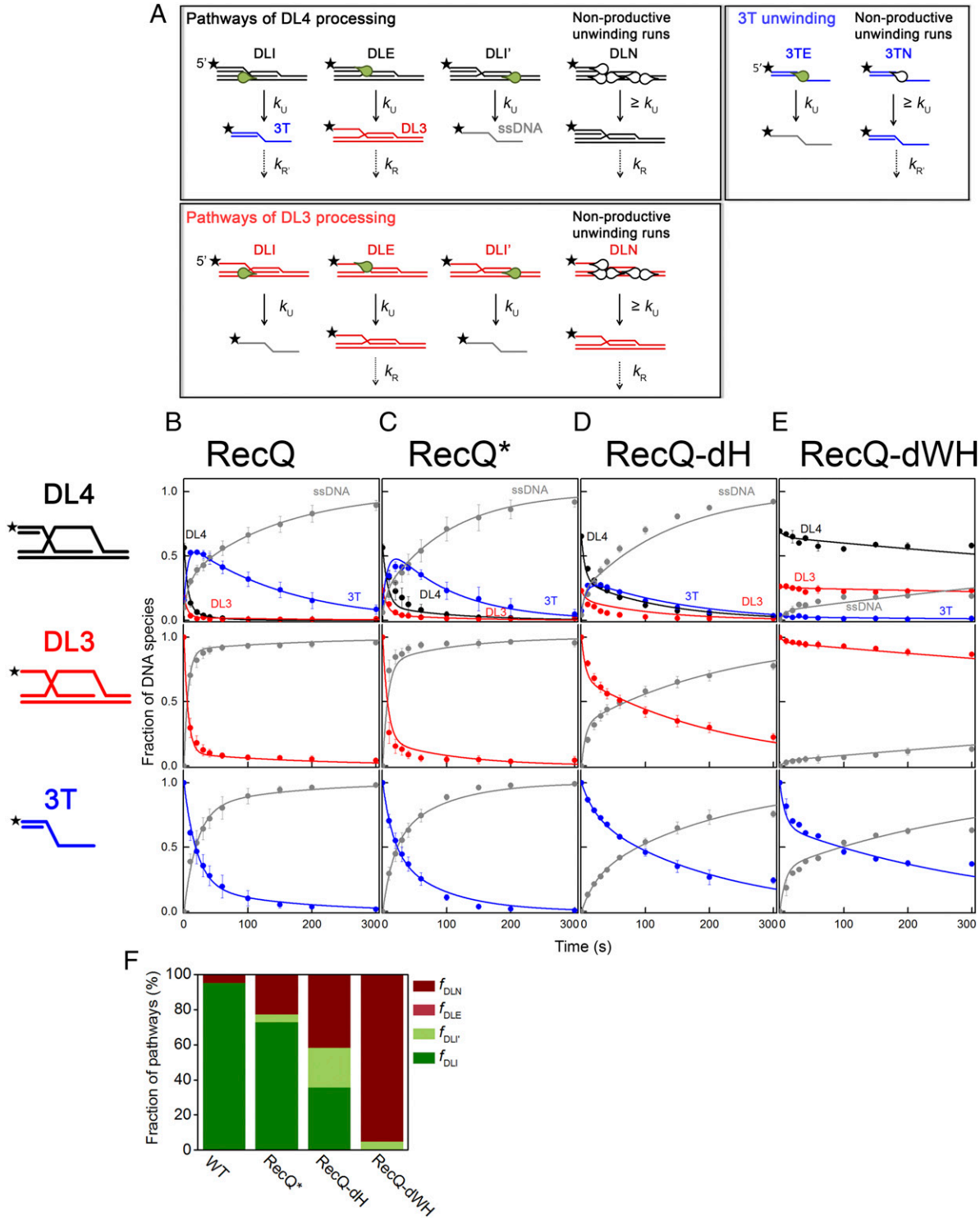

Fig. 2. The WHD and HRDC domains enable directed processing of D-loop structures. (*A*) Pathways of processing of D-loop–like (four-stranded DL4, black; three-stranded DL3, red) and 3′-tailed (3T, blue) DNA substrates. DNA-bound helicases are shown as green drops pointing in the direction of unwinding (3′–5′ on the tracked DNA strand). Black stars represent the Cy3 fluorescent label at the 5′ end of the invading DNA strand. Enzyme–DNA complexes are initially distributed into different configurations (DLI, DLE, DLI′, DLN; 3TE, 3TN; as described in the text). DLN and 3TN represent all nonproductive unwinding runs starting from any possible enzyme–DNA configuration (white drops; see text). Unwinding (occurring at rate constant k_U) leads to the indicated DNA products. Slow rebinding of enzyme to these DNA products (inhibited by excess ssDNA trap strand, occurring at k_R for DL4 and DL3, or k_R' for 3T) leads to reformation of enzyme–DNA configurations (with the same distribution as for the initial complexes; reformation and redistribution together are indicated by downward arrows labeled k_R and k_R'). (*B–E*) Kinetic profiles of DL4, DL3, and 3T unwinding by RecQ (*B*), RecQ* (*C*), RecQ-dH (*D*), and RecQ-dWH (*E*) [100 nM enzyme, except that 3 μM RecQ-dWH was used in *E*, 30 nM labeled DNA, 3 μM ssDNA trap strand; means ± SE ($n = 5$ for DL4, $n = 3$ for DL3 and 3T) are shown; see also Figs. S6 and S7]. Color code of DNA species is as in *A*. Solid lines show global best fits to all unwinding data (DL4, DL3, and 3T) of each enzyme variant. (*F*) Distributions of enzyme-DL (DL4 or DL3) configurations resulting from global fits shown in *B–E*. Determined parameters are listed in Table S1. DNA substrates are described in Table S2.

The decrease in the disrupted fraction (DLI+DLI′) observed for the HRDC and combined WHD-HRDC deletion constructs reflects the contribution of both domains to the disruption of invasions by RecQ (Fig. 2*F*). Furthermore, the HRDC domain of RecQ confers a strong bias toward the DLI configuration, and this effect is largely independent of the ssDNA binding capability of this domain (RecQ, RecQ*, and RecQ-dH data in Fig. 2*F*). In experiments measuring the affinity of RecQ enzyme constructs and isolated (WT and Y555A mutant) HRDC domains for the DNA substrates, we ruled out the possibility that the HRDC domain specifically binds branched DNA structures independent of its ssDNA binding capability (Figs. S7 and S8).

Figs. S6–S8 and Table S1 show results of control experiments verifying the kinetic analysis of the D-loop DNA disruption experiments.

Activities Mediated by the HRDC Domain Suppress Illegitimate Recombination in Vivo. To assess the physiological effects of HRDC and WHD mutations, we created *E. coli* strains (based on MG1655 used as WT) lacking RecQ (Δ*recQ*), or expressing the characterized point mutant (*recQ**) or truncated forms (*recQ-dH*, *recQ-dWH*) in place of the WT protein (Table S3). The growth curves of WT, *recQ**, and *recQ-dH* strains were similar, whereas Δ*recQ* and *recQ-dWH* showed slightly slower growth at the end of log phase (Fig. 3*A*). We characterized the genome damage tolerance of the strains via UV irradiation and nitrofurantoin (NIT) survival assays (Fig. 3 *B* and *C*, and Table S4). UV irradiation induces the formation of pyrimidine dimers, whereas NIT introduces interstrand cross-links in DNA (27, 28). Both forms of DNA damage can halt DNA replication if unrepaired. With the exception of *recQ-dWH*, we found no significant effects of *recQ* mutations on the UV sensitivity of *E. coli* strains (Fig. 3*B* and Table S4).

An antibiotic sensitivity screen of single-gene knockout *E. coli* strains showed that the Δ*recQ* mutation selectively increased NIT sensitivity (29). We found that NIT exerts a toxic effect even on WT, *recQ**, and *recQ-dH* cells with a very high apparent cooperativity (Fig. 3*C* and Table S4). Consistent with a previous study (29), we found significantly increased NIT sensitivity for Δ*recQ* compared with WT. A similar increased NIT sensitivity was observed for *recQ-dWH* (Fig. 3*C* and Table S4).

The Spi$^-$ λ phage assay allows quantification of illegitimate recombination frequencies (IRFs) (30, 31). Upon lytic phase induction, λ phage is normally excised from the genome of lysogenic strains by site-specific recombination. IR events produce phage variants that lack the *red* and *gam* genes and therefore, unlike the WT phage, are able to form plaques on P2 lysogenic *E. coli* strains (Spi$^-$ phenotype). We found that, in the absence of UV irradiation, all mutant strains showed elevated IRF values compared with WT (Fig. 3*D* and Table S4). UV irradiation markedly increased the IRF in WT, consistent with previous findings (22, 31). The UV-induced IRF values of Δ*recQ*, *recQ-dWH*, and *recQ** were elevated compared with that of WT, whereas *recQ-dH* exhibited an even higher IRF value (Fig. 3*D* and Table S4). Reported differences are statistically significant ($P < 0.05$) based on two-tailed *t* test statistics. More stringent ANOVA analysis of log-transformed IRF values (performed based on log-normal distribution of IRF), followed by the Tukey post hoc test, demonstrated that the UV-free IRF values of Δ*recQ*, *recQ-dWH*, and *recQ-dH*, and the UV-induced IRF of *recQ** and *recQ-dH* were significantly higher than the corresponding WT values ($P < 0.05$) (Fig. 3*D*). These results show that in vivo IR suppression by RecQ is compromised by the abolition of activities conferred by the HRDC and WHD domains.

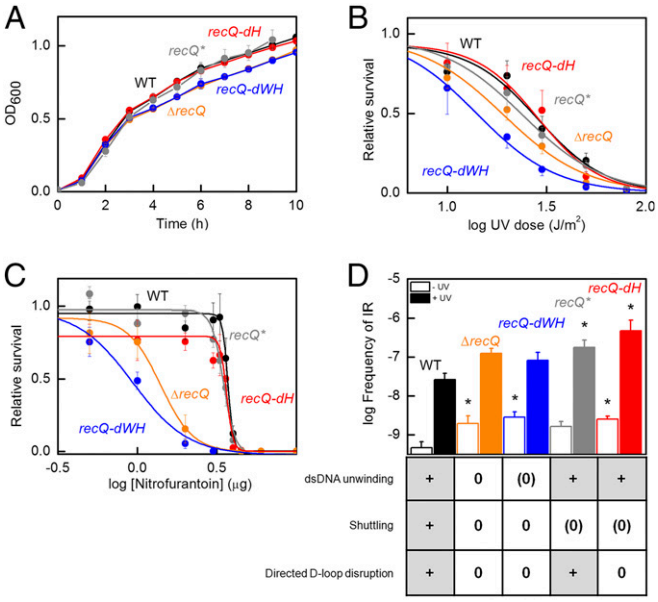

Fig. 3. Shuttling and directed D-loop disruption activities are required to suppress illegitimate recombination in *E. coli*. (*A*) Growth curves of MG1655 (WT), Δ*recQ*, *recQ**, *recQ-dH*, and *recQ-dWH E. coli* strains. (*B* and *C*) Dose-dependent survival curves of *E. coli* strains exposed to UV irradiation (*B*) or NIT (*C*). Solid lines in *B* and *C* show fits to averaged data based on a standard dose–response model (Eq. S6). (*D*) Frequencies of illegitimate recombination (IR) in *E. coli* strains (log-transformed values), as determined using the λ phage Spi$^-$ assay, with or without UV irradiation (50 J/m^2). Asterisks indicate significant difference from WT values ($P < 0.05$, one-way ANOVA followed by Tukey test). The table shows in vitro activities of RecQ constructs expressed by the individual strains, as determined in biophysical experiments. +, activity present; 0, activity absent; (0), weak activity. Statistics of parameters determined for individual datasets are shown in Table S4.

Discussion

Single-molecule and ensemble measurements revealed a striking DNA geometry-dependent unwinding behavior for *E. coli* RecQ (Figs. 1 and 2). Unwinding of gapped DNA, similar to DNA resection, was comparable for all RecQ constructs. Unwinding of hairpin DNA, similar in some respects to disruption of homologous paired DNA, was dramatically different for the RecQ constructs in which the HRDC domain was mutated or deleted. Unwinding behavior at the end of the DNA hairpin, although not obviously analogous to physiological DNA structures, provided additional mechanistic insights into the functions of the specific domains and their interactions. Based on these observations, we propose a mechanistic model in which shuttling and directed D-loop processing activities arise from an interplay between the dynamic interactions of the HRDC domain and the substrate preference of the WHD (Fig. 4).

In the proposed model, the WHD acts as a processivity factor through its stabilizing interactions with dsDNA ahead of the progressing helicase core (state 1 in Fig. 4*A*). This role is consistent with the decrease in processivity and DNA binding that accompanies deletion of the WHD (RecQ-dWH; Fig. 1; Figs. S1, S2, and S5; Table 1; Tables S1 and S5). Accordingly, a WHD is present in many nucleic acid binding proteins in which it is typically implicated in binding ds nucleic acids (6). In line with the diversity of their cellular roles, RecQ family members show considerable variation regarding the presence and functional role of the WHD and HRDC domains (32). A β-hairpin within the WHD is an essential DNA unwinding wedge in human RECQ1 helicase (33). However, the corresponding region of *E. coli* RecQ is dispensable for unwinding activity (33), and the entire WHD of human BLM was found to be dispensable for DNA binding and unwinding (34). Our results with RecQ-dWH show that the WHD is dispensable for individual unwinding steps per se, but that it facilitates processive dsDNA unwinding (Figs. 1 and 2, Fig. S2, Table 1, and Table S1). Consistent with this interpretation, deletion of the WHD drastically

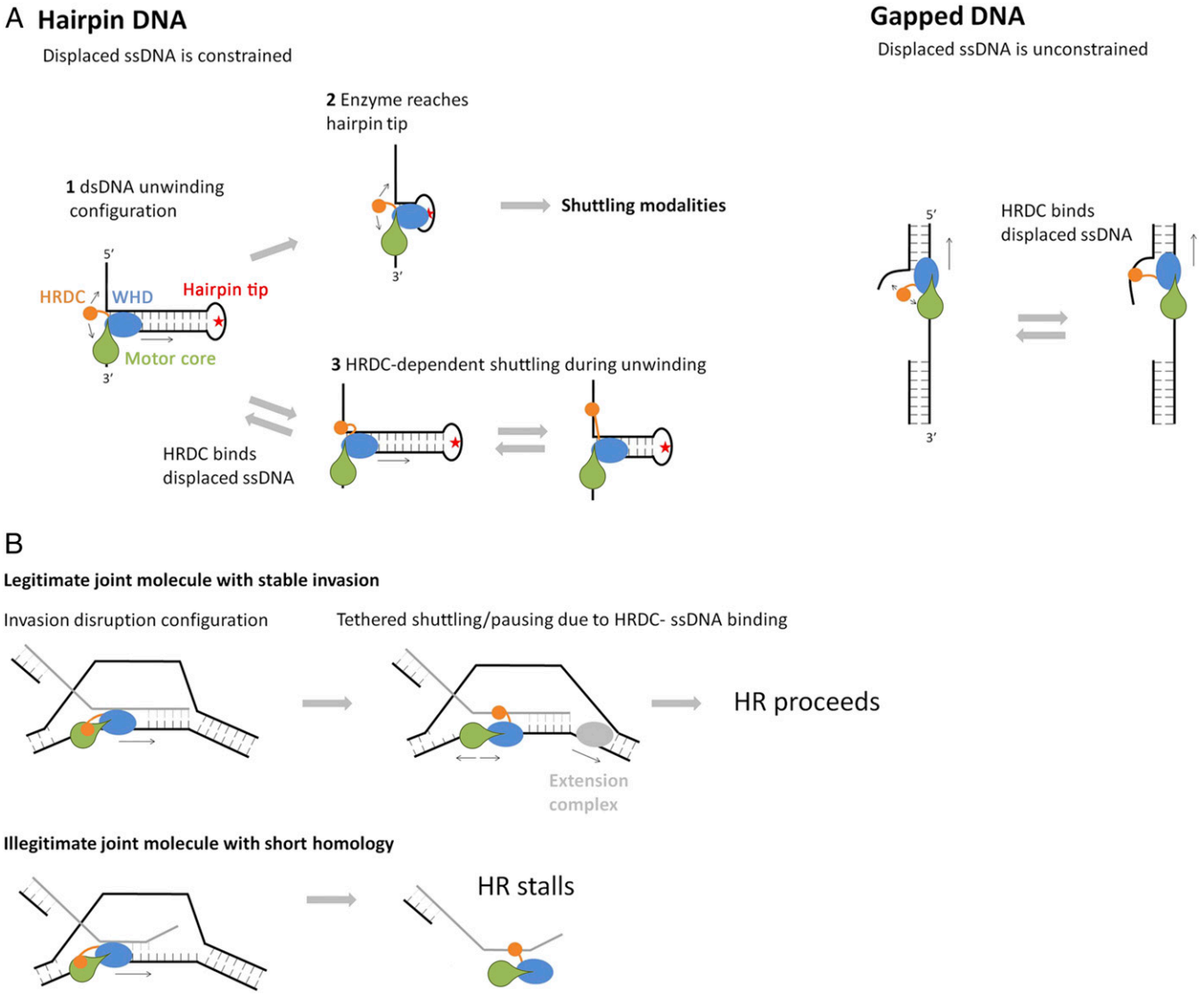

Fig. 4. DNA geometry-dependent activities of RecQ helicases and their contribution to recombination quality control. (*A*) Model illustrating key differences between DNA geometries (hairpin DNA, *Left*; gapped DNA, *Right*) and shuttling events occurring during unwinding and upon reaching the tip of the hairpin DNA substrate. During dsDNA unwinding (state 1), the WHD (blue oval) is bound to the dsDNA segment ahead of the progressing helicase core (green drop), whereas the HRDC domain (orange circle) can form transient interactions with the displaced ssDNA strand, thereby inducing shuttling on hairpin DNA (state 3). At the hairpin end (Figs. S1 and S9), additional shuttling modalities can be observed. On gapped DNA, HRDC–ssDNA interactions do not hinder the progression of the helicase core, which unwinds DNA processively without shuttling or pausing. (*B*) RecQ helicase preferentially binds to D-loops in an orientation favoring invasion disruption (left panels, configuration "DLI" in Fig. 2*A*, facilitated by HRDC–motor core interactions). During DNA unwinding, HRDC-dependent pausing and shuttling activities hinder the disruption of stable, long invasions occurring during legitimate recombination, thereby enabling HR progression (upper row). However, short homologous regions, characteristic of illegitimate recombination, are unwound rapidly, thus reducing the probability of HRDC-induced pausing and shuttling. This mechanism thus aids quality control by selective disruption of illegitimate invasions.

reduced the affinity of RecQ for various DNA substrates (Figs. S5 and S7, Table 1, and Table S1).

During dsDNA unwinding (states 1–2 in Fig. 4*A*), the HRDC domain may interact transiently with the displaced ssDNA strand (arrows in state 1). This results in frequent and long pauses that are often accompanied by short-extent, long-duration shuttling of RecQ on hairpin DNA (state 3 in Fig. 4*A*). This behavior is pronounced for RecQ at the end of the DNA hairpin, along with other shuttling modalities (see Figs. S1 and S9 for a possible mechanistic scheme for different shuttling modalities). Shuttling, and in particular short-extent, long-duration shuttling, was significantly reduced in the HRDC point (RecQ*) and deletion (RecQ-dH) mutants, and during gapped DNA unwinding by all constructs (Fig. 1, Fig. S1, and Table 1). Whereas the HRDC domain is dispensable for strong DNA binding (Figs. S2, S5, and S7, Table 1, and Tables S1 and S5), its transient interactions with ssDNA reduce the processivity and mean rate of hairpin DNA unwinding (Fig. 1, Fig. S2, and Table 1). In addition, the HRDC domain suppresses the ATPase activity of *E. coli* RecQ (Fig. S5 and Table 1), most likely through interactions with the motor core, as has been observed in recent BLM crystal structures (26, 35).

In addition to inducing shuttling during dsDNA hairpin unwinding, we found that the HRDC domain increased the efficiency of D-loop disruption, that is, oriented unwinding of the invading ssDNA strand, even when its ssDNA binding capability was abolished (by the Y555A mutation in RecQ*) (Fig. 2, Figs. S5 and S7, Table 1, and Table S1). These results (Fig. 2*F*) suggest that efficient D-loop disruption is achieved through the initial binding of the

helicase in an orientation that leads to unwinding of the invading strand (configuration DLI in Fig. 2*A*; Fig. 4*B*), rather than unwinding the intact dsDNA segments, which would promote invasion (configurations DLE and DLN in Fig. 2*A*). Our results showed that the isolated HRDC domain interacts with the branched region of D-loops by binding ssDNA rather than a structure specific interaction (Fig. S8). These findings raise the possibility that the HRDC–motor core interaction stabilizes the helicase in a configuration specific for invasion disruption (36) (Fig. 4*B*).

Taken together, our results show that the conserved RecQ domain architecture supports sensing of DNA geometry during DNA-restructuring reactions and effects complex responses to enzyme-induced changes in substrate geometry. Below, we propose how these mechanisms may support recombination quality control.

Bacterial and eukaryotic RecQ helicases participate in several DNA repair and replication restart pathways in which they perform distinct functions (5). In *E. coli*, RecQ functions as a canonical helicase unwinding dsDNA in the RecF HR pathway and during replication restart (37, 38). However, RecQ also disrupts D-loops and, in conjunction with topoisomerase III, resolves converging replication forks (8, 39). Consistent with this functional diversity, we found that *E. coli* strains lacking RecQ helicase activity (Δ*recQ*, *recQ-dWH*) exhibited a modest decrease in DNA damage tolerance, whereas strains expressing RecQ helicase variants with altered or deleted HRDC domains (*recQ**, *recQ-dH*) exhibited WT-like damage tolerance (Fig. 3 *B* and *C*, and Table S4).

A cardinal function of RecQ helicases is the suppression of potentially harmful IR, that is, recombination occurring between nonallelic DNA segments (1), which can be initiated from locally base-paired intermediates (31). RecQ-catalyzed disruption of these structures effectively suppresses IR (31). Accordingly, we found that Δ*recQ* and *recQ-dWH E. coli* strains showed elevated IRF compared with WT (Fig. 3*D*). Strikingly, we found that replacing WT RecQ with the HRDC-deletion construct (*recQ-dH* strain) markedly elevated IRF to levels well above those in the Δ*recQ*-null strain (Fig. 3*D*). This finding, combined with the fact that the *recQ-dH* strain shows a WT-like DNA damage repair phenotype (Fig. 3 *A*–*C*), indicates that the HRDC domain exerts control over the helicase core to promote disruption of IR despite the apparent tendency of the HRDC-less enzyme to enhance IR. Interestingly, the *recQ** strain also shows higher IRF than WT (Fig. 3*D*) even though the efficiency of in vitro D-loop disruption by RecQ* was comparable to that of RecQ (Fig. 2*F*). This suggests that processive dsDNA unwinding facilitated by the WHD without the HRDC-induced pausing and shuttling appears to promote IR, likely due to the generation of ssDNA segments that can lead to illegitimate base pairing combined with the elevated probability of extending rather than disrupting the resulting short D-loop–like structures (Figs. 2 and 4*B*) (22). Conversely, the HRDC-mediated increase in the precision of HR events likely arises from the ability of RecQ to preferentially and specifically reverse ssDNA strand invasion of duplex DNA and disrupt D-loop–like structures (Figs. 2 and 4*B*), which are early recombination intermediates. In this scenario, RecQ preferentially disrupts illegitimate, D-loop–like structures that can form spontaneously between short homologous regions, similar to those in our D-loop–like structures that were preferentially disrupted by RecQ (Figs. 2 and 4*B*). Short homologous regions are unwound rapidly as HRDC-mediated shuttling is infrequent in this length range (Fig. 4*B*). In contrast, legitimate invasions are longer, more stable, and/or specifically stabilized by additional factors. During unwinding of long invasions, HRDC-mediated pausing and shuttling occur with a high probability and halt D-loop disruption for extended periods of time (shuttling duration in Table S1). This mechanism may create an opportunity for organization of protein complexes to extend the D-loop and promote HR (Fig. 4*C*). Thus, based on our model, both HRDC-mediated shuttling and directed D-loop disruption jointly contribute to quality control of HR via selective disruption of IR intermediates (Fig. 3*D* and Table S4). This model is supported by the marked increase in IRF for the *recQ-dH E. coli* strain expressing RecQ lacking the HRDC domain (Fig. 3*D*). The lack of the HRDC-mediated shuttling activity, together with the lack of directed disruption of strand invasions, renders RecQ-dH much less effective in the disruption of short base-paired intermediates, and may in fact promote strand invasion in vivo.

Taken together, these findings underscore the importance of the auxiliary DNA binding domains in sensing and response to DNA geometry during DNA-processing reactions. In addition to providing a mechanistic explanation of the observed behavior of RecQ, our model has broad implications for nucleic acid-based motor enzymes more generally. (*i*) The presence of a dsDNA-binding domain attached to the helicase core, that is, the WHD in RecQ enzymes, is sufficient to elicit a complex, repetitive unwinding behavior involving strand switching. Strand switching is a common feature among many SF1 and SF2 helicases containing at least one auxiliary dsDNA-binding domain (40–42). An additional ssDNA-binding element, that is, the HRDC domain, adds further complexity to repetitive unwinding via dynamic, multipartite interactions. (*ii*) The model implies large-scale reorientation of protein domains and/or changes in DNA conformation. Such changes have been demonstrated for several SF1 helicases (43, 44), and recent studies suggest that the mobility of the WH and HRDC domains is a general feature of RecQ helicases (26, 33, 35, 45, 46).

Materials and Methods

Magnetic-Tweezers Experiments. The DNA hairpin substrate was attached to the flow cell surface and to a 2.8-μm magnetic bead via a 1-kbp dsDNA handle and 60 nt of poly-dT, respectively. Attachment was performed as follows. The 0.3 nM DNA was incubated with 32 ng of anti-digoxigenin in 50 μL of 1× PBS, pH 7.4 (Invitrogen), for 1 h at room temperature. This mixture was introduced into a sample cell coated with a low concentration of stuck beads and incubated overnight at 4 °C. Unbound DNA was washed out with 200 μL of wash buffer [PBS supplemented with 0.04% (vol/vol) Tween 20 and 0.3% (wt/vol) BSA]. Twenty microliters of 20× dilution of streptavidin-coated magnetic beads (MyOne; Invitrogen) were then introduced in wash buffer and allowed to tether for 1 h and washed with 1 mL of wash buffer. Once a proper DNA substrate was found based on contour length and extension change due to force-dependent dsDNA opening, the chamber was washed with 200 μL of RecQ buffer [30 mM Tris, pH 8, 50 mM NaCl, 5 mM $MgCl_2$, 0.3% (wt/vol) BSA, 0.04% (vol/vol) Tween 20, and 1 mM DTT]. After washing, RecQ constructs were added at a concentration of 50 pM (except for RecQ-dWH, 500 pM) in 200 μL of RecQ buffer supplemented with 1 mM ATP. Measurements with the DNA hairpin were performed at a constant force of 8 pN under which the hairpin did not open spontaneously. In the presence of RecQ helicases and saturating ATP (1 mM), unwinding activity was monitored in real time by tracking the 3D position of a tethered bead at 60 or 200 Hz using image analysis software, simultaneously tracking a stuck bead for drift correction. Conversion of the measured change in extension to the number of DNA base pairs unzipped was done based on the worm-like chain model of ssDNA (47). Measurements with the gapped DNA substrate were performed at a constant force of 15 pN. The change in extension associated with the transition from dsDNA to ssDNA provided a measure of helicase unwinding activity. Typical unwinding records contained multiple unwinding events defined as the opening of the DNA hairpin by the helicase (when the extension exceeded 3 SDs of the baseline Brownian noise measured when no unwinding occurs) to the full reannealing of DNA hairpin back to the baseline (Fig. 1*C*). The total number of events for individual enzymes are reported in Table 1. Trajectories of the bead extension as a function of time were analyzed by fitting with a *t* test-based step-finding algorithm to obtain the mean unwinding rate, the step unwinding rate between pauses, the pause positions, and the pause durations (48). The mean rate was calculated by linear fits ranging from the initial unwinding position to the maximum unwinding position before the helicase dissociated or the hairpin rezipped. The step rate corresponds to the unwinding rate between pauses obtained from fitting the trajectories with a step-finding algorithm.

DNA substrate preparation and additional controls for magnetic tweezers experiments can be found in *SI Materials and Methods* and Figs. S10–S12.

Solution Kinetic DNA Unwinding Experiments. DNA substrates (30 nM; final reaction concentrations stated) were incubated with excess enzyme (100 nM, unless otherwise stated) at 4 °C for 10 min, and then at 37 °C for 3 min in Buffer H (30 mM Tris·HCl, pH 7.5, 100 mM KCl, 1 mM DTT, 50 μg/mL BSA, 20 mM creatine phosphate, 20 μg/mL creatine kinase). Reactions were started at 37 °C by mixing the DNA–enzyme complex with Buffer H containing ATP (3 mM), $MgCl_2$ (3 mM), and ssDNA trap strand (3 μM, unless otherwise stated) to inhibit enzyme rebinding to DNA. Reactions were stopped manually after preset reaction times by the addition of EDTA (40 mM final, pH 8.1) and loading dye [10 mM Tris·HCl, pH 7.5, 40 mM EDTA, 60% (vol/vol) glycerol, 0.075% (wt/vol) Orange G, 0.83% (wt/vol) SDS]. Mixtures were incubated at 37 °C for additional 3 min. Samples were then loaded on 12% (wt/vol) nondenaturing polyacrylamide gels in TBE buffer (89 mM Tris·HCl, pH 7.5, 89 mM boric acid, 20 mM EDTA). Electrophoresis was carried out at 4 °C. Cy3-labeled DNA was detected by using a Typhoon TRIO+ Variable Mode Imager (Amersham Biosciences). The intensities of bands corresponding to the DNA substrate and unwinding products were quantified by densitometry.

Cell Growth and Survival Assays. Growth curves were recorded by inoculating aliquots of overnight *E. coli* cultures into Luria–Bertani (LB) medium to an OD_{600} of 0.01, followed by incubation at 37 °C with aeration and monitoring their OD_{600} value. In UV irradiation survival assays, cells were grown to 4×10^8 cells per mL at 37 °C in LB medium. Aliquots of cultures were diluted 10^6-fold, spread onto LB plates, and irradiated with different UV doses (at 254 nm) using an UVP CX-2000 cross-linker. Following irradiation and overnight growth at 37 °C, colonies were counted to quantify survival. NIT survival assays were performed as described for UV survival assays, except that UV irradiation was omitted and cells were spread and grown on LB plates containing different concentration of NIT. Dimethylformamide (used as solvent in NIT stock solutions) was applied in control plates at a concentration identical to NIT-containing plates (0.06%).

Spi⁻ Phage Assay for Illegitimate Recombination. The frequency of illegitimate recombination of λ phage was measured using the λ Spi⁻ assay developed by Ikeda and coworkers (31). For lysogenization, WT and *recQ* mutant *E. coli* cells were grown to 7×10^8 cells per mL at 30 °C in T-broth [1% bacto tryptone (Difco), 0.5% NaCl, 10 mM $MgSO_4$, 0.2% maltose]. λcI857 phage, isolated from HI1165 cells after heat shock induction of lytic phase, was added to WT and *recQ* mutant *E. coli* cells (at multiplicity of infection of 2) and incubated for 30 min at 30 °C. Cells were then spread onto T-plates [T-broth with 1.2% (wt/vol) agar] and incubated at 30 °C overnight. Single colonies were picked, amplified, and checked for lysogeny by heat shock induction of lytic phase [42 °C for 15 min, followed by shaking (250 rpm, Innova 44 shaker incubator, New Brunswick Co., Edison, NJ) at 37 °C and monitoring decrease in OD_{600}]. To analyze the formation of λ Spi⁻ phages, lysogenic strains (Table S3) were grown to 4×10^8 cells per mL in λYP broth [1% bacto tryptone (Difco), 0.1% yeast extract (Oxoid), 0.25% NaCl, 0.15% $NaHPO_4$, 0.018% $MgSO_4$]. When applicable, 5 mL of the culture was irradiated at room temperature with UV light at a dose of 50 J/m² using a UVP CX-2000 cross-linker. To enter the lytic phase, λcI857 prophage was heat induced by incubation of the culture at 42 °C for 15 min. The culture was then incubated at 37 °C for 2 h with aeration and centrifuged to isolate the phages from cell debris. The total phage titer and the titer of λ Spi⁻ phages was determined by phage infection of YmeI and WL95 (P2 lysogen) *E. coli* cells, respectively (Table S3). Mixtures of (diluted) aliquots of the phage suspension and YmeI or WL95 cells were incubated at room temperature for 30 min, mixed with λ top agar (1% bacto tryptone, 0.5% NaCl, 0.4% agar; for YmeI) or λ trypticase top agar [1% trypticase peptone (Difco), 0.5% NaCl, 0.4% agar; for WL95] and spread onto 1.2% (wt/vol) agar plates (otherwise identical to the respective top agar). Plaques were counted after overnight incubation at 37 °C. The burst size, calculated by dividing the titer of total phages by the titer of infective centers, was in the range of 18–82. The IRF was obtained by dividing the titer of λ Spi⁻ phages by the titer of total phage.

Data Analysis. Means ± SE values are reported in the paper, unless otherwise specified. Sample sizes (n) are given for (*i*) number of observed events in magnetic-tweezers experiments, (*ii*) number of ensemble in vitro measurements performed using independent protein preparations (biological replicates; $n = 3$, unless otherwise specified), (*iii*) number of experiments performed using independent bacterial colonies (biological replicates). Data analysis was performed using OriginLab 8.0 (Microcal) and GelQuant Pro software (DNR Bio Imaging). Magnetic-tweezers data traces were analyzed using a custom step-finding program written in Igor Pro (WaveMetrics) (49). Global-fitting kinetic analysis was performed using KinTek Global Kinetic Explorer 4.0, based on mass action rate equations accounting for all steps depicted in Fig. 2*A*, and the initial fractions of the DNA species shown at zero time in Fig. 2 *B–E* and Fig. S6*E* (50).

Further descriptions of materials and methods can be found in *SI Materials and Methods*.

ACKNOWLEDGMENTS. We are grateful to Dr. Marie-Paule Strub for assistance with protein expression and purification, Dr. Duck-Yeon Lee (National Heart, Lung, and Blood Institute Biochemistry Core) for assistance with mass spectroscopy, and Drs. Hideo Ikeda and Yasuyuki Ogata for providing the YmeI, WL95, and HI1165 *E. coli* strains. This work was supported by Human Frontier Science Program Grant RGY0072/2010 (to M.K. and K.C.N.); Hungarian Academy of Sciences "Momentum" Program Grant LP2011-006/2011 (to M.K.); Eötvös Loránd University Grant KMOP-4.2.1/B-10-2011-0002; National Research, Development and Innovation Office (NKFIH) Grant K-116072; and NKFIH Grant ERC_HU 117680 (to M.K.). This work was supported in part by National Heart, Lung, and Blood Institute, National Institutes of Health, Intramural Research Program Grant HL001056-07 (to K.C.N.). M.G. is supported by Marie Sklodowska-Curie Reintegration Fellowship H2020-MSCA-IF-2014-657076.

1. Brosh RM, Jr (2013) DNA helicases involved in DNA repair and their roles in cancer. *Nat Rev Cancer* 13(8):542–558.
2. Bell JC, Kowalczykowski SC (2016) Mechanics and single-molecule interrogation of DNA recombination. *Annu Rev Biochem* 85:193–226.
3. Chu WK, Hickson ID (2009) RecQ helicases: Multifunctional genome caretakers. *Nat Rev Cancer* 9(9):644–654.
4. Singh DK, Ghosh AK, Croteau DL, Bohr VA (2012) RecQ helicases in DNA double strand break repair and telomere maintenance. *Mutat Res* 736(1-2):15–24.
5. Bernstein KA, Gangloff S, Rothstein R (2010) The RecQ DNA helicases in DNA repair. *Annu Rev Genet* 44:393–417.
6. Harami GM, Gyimesi M, Kovács M (2013) From keys to bulldozers: Expanding roles for winged helix domains in nucleic-acid-binding proteins. *Trends Biochem Sci* 38(7):364–371.
7. van Brabant AJ, et al. (2000) Binding and melting of D-loops by the Bloom syndrome helicase. *Biochemistry* 39(47):14617–14625.
8. Harmon FG, Kowalczykowski SC (1998) RecQ helicase, in concert with RecA and SSB proteins, initiates and disrupts DNA recombination. *Genes Dev* 12(8):1134–1144.
9. Klaue D, et al. (2013) Fork sensing and strand switching control antagonistic activities of RecQ helicases. *Nat Commun* 4:2024.
10. Yodh JG, Stevens BC, Kanagaraj R, Janscak P, Ha T (2009) BLM helicase measures DNA unwound before switching strands and hRPA promotes unwinding reinitiation. *EMBO J* 28(4):405–416.
11. Wang S, et al. (2015) Unwinding forward and sliding back: An intermittent unwinding mode of the BLM helicase. *Nucleic Acids Res* 43(7):3736–3746.
12. Wu L, et al. (2005) The HRDC domain of BLM is required for the dissolution of double Holliday junctions. *EMBO J* 24(14):2679–2687.
13. Bernstein DA, Keck JL (2005) Conferring substrate specificity to DNA helicases: Role of the RecQ HRDC domain. *Structure* 13(8):1173–1182.
14. Chatterjee S, et al. (2014) Mechanistic insight into the interaction of BLM helicase with intra-strand G-quadruplex structures. *Nat Commun* 5:5556.
15. Hishida T, et al. (2004) Role of the *Escherichia coli* RecQ DNA helicase in SOS signaling and genome stabilization at stalled replication forks. *Genes Dev* 18(15):1886–1897.
16. Kocsis ZS, Sarlós K, Harami GM, Martina M, Kovács M (2014) A nucleotide-dependent and HRDC domain-dependent structural transition in DNA-bound RecQ helicase. *J Biol Chem* 289(9):5938–5949.
17. Harami GM, Nagy NT, Martina M, Neuman KC, Kovács M (2015) The HRDC domain of *E. coli* RecQ helicase controls single-stranded DNA translocation and double-stranded DNA unwinding rates without affecting mechanoenzymatic coupling. *Sci Rep* 5:11091.
18. Cheng W, Dumont S, Tinoco I, Jr, Bustamante C (2007) NS3 helicase actively separates RNA strands and senses sequence barriers ahead of the opening fork. *Proc Natl Acad Sci USA* 104(35):13954–13959.
19. Qi Z, Pugh RA, Spies M, Chemla YR (2013) Sequence-dependent base pair stepping dynamics in XPD helicase unwinding. *eLife* 2:e00334.
20. Carter AR, et al. (2016) Sequence-dependent nanometer-scale conformational dynamics of individual RecBCD-DNA complexes. *Nucleic Acids Res* 44(12):5849–5860.
21. Morimatsu K, Kowalczykowski SC (2014) RecQ helicase and RecJ nuclease provide complementary functions to resect DNA for homologous recombination. *Proc Natl Acad Sci USA* 111(48):E5133–E5142.
22. Ivanković S, Đermić D (2012) DNA end resection controls the balance between homologous and illegitimate recombination in *Escherichia coli*. *PLoS One* 7(6):e39030.
23. Gyimesi M, Sarlós K, Kovács M (2010) Processive translocation mechanism of the human Bloom's syndrome helicase along single-stranded DNA. *Nucleic Acids Res* 38(13):4404–4414.
24. Sarlós K, Gyimesi M, Kovács M (2012) RecQ helicase translocates along single-stranded DNA with a moderate processivity and tight mechanochemical coupling. *Proc Natl Acad Sci USA* 109(25):9804–9809.
25. Gyimesi M, Harami GM, Kocsis ZS, Kovács M (2016) Recent adaptations of fluorescence techniques for the determination of mechanistic parameters of helicases and translocases. *Methods* 108:24–39.

26. Swan MK, et al. (2014) Structure of human Bloom's syndrome helicase in complex with ADP and duplex DNA. *Acta Crystallogr D Biol Crystallogr* 70(Pt 5):1465–1475.
27. Yang W (2011) Surviving the sun: Repair and bypass of DNA UV lesions. *Protein Sci* 20(11):1781–1789.
28. Mukherjee U, Basak J, Chatterjee SN (1990) DNA damage and cell killing by nitrofurantoin in relation to its carcinogenic potential. *Cancer Biochem Biophys* 11(4): 275–287.
29. Liu A, et al. (2010) Antibiotic sensitivity profiles determined with an *Escherichia coli* gene knockout collection: Generating an antibiotic bar code. *Antimicrob Agents Chemother* 54(4):1393–1403.
30. Ikeda H, Shimizu H, Ukita T, Kumagai M (1995) A novel assay for illegitimate recombination in *Escherichia coli*: Stimulation of lambda bio transducing phage formation by ultra-violet light and its independence from RecA function. *Adv Biophys* 31:197–208.
31. Hanada K, et al. (1997) RecQ DNA helicase is a suppressor of illegitimate recombination in *Escherichia coli*. *Proc Natl Acad Sci USA* 94(8):3860–3865.
32. Vindigni A, Hickson ID (2009) RecQ helicases: Multiple structures for multiple functions? *HFSP J* 3(3):153–164.
33. Pike ACW, et al. (2009) Structure of the human RECQ1 helicase reveals a putative strand-separation pin. *Proc Natl Acad Sci USA* 106(4):1039–1044.
34. Gyimesi M, et al. (2012) Complex activities of the human Bloom's syndrome helicase are encoded in a core region comprising the RecA and Zn-binding domains. *Nucleic Acids Res* 40(9):3952–3963.
35. Newman JA, et al. (2015) Crystal structure of the Bloom's syndrome helicase indicates a role for the HRDC domain in conformational changes. *Nucleic Acids Res* 43(10): 5221–5235.
36. Kitano K (2014) Structural mechanisms of human RecQ helicases WRN and BLM. *Front Genet* 5:366.
37. Handa N, Morimatsu K, Lovett ST, Kowalczykowski SC (2009) Reconstitution of initial steps of dsDNA break repair by the RecF pathway of *E. coli*. *Genes Dev* 23(10): 1234–1245.
38. Kuzminov A (1999) Recombinational repair of DNA damage in *Escherichia coli* and bacteriophage lambda. *Microbiol Mol Biol Rev* 63(4):751–813.
39. Suski C, Marians KJ (2008) Resolution of converging replication forks by RecQ and topoisomerase III. *Mol Cell* 30(6):779–789.
40. Dessinges MN, Lionnet T, Xi XG, Bensimon D, Croquette V (2004) Single-molecule assay reveals strand switching and enhanced processivity of UvrD. *Proc Natl Acad Sci USA* 101(17):6439–6444.
41. Myong S, Bruno MM, Pyle AM, Ha T (2007) Spring-loaded mechanism of DNA unwinding by hepatitis C virus NS3 helicase. *Science* 317(5837):513–516.
42. Myong S, Rasnik I, Joo C, Lohman TM, Ha T (2005) Repetitive shuttling of a motor protein on DNA. *Nature* 437(7063):1321–1325.
43. Velankar SS, Soultanas P, Dillingham MS, Subramanya HS, Wigley DB (1999) Crystal structures of complexes of PcrA DNA helicase with a DNA substrate indicate an inchworm mechanism. *Cell* 97(1):75–84.
44. Lee JY, Yang W (2006) UvrD helicase unwinds DNA one base pair at a time by a two-part power stroke. *Cell* 127(7):1349–1360.
45. Bernstein DA, Zittel MC, Keck JL (2003) High-resolution structure of the *E. coli* RecQ helicase catalytic core. *EMBO J* 22(19):4910–4921.
46. Manthei KA, Hill MC, Burke JE, Butcher SE, Keck JL (2015) Structural mechanisms of DNA binding and unwinding in bacterial RecQ helicases. *Proc Natl Acad Sci USA* 112(14):4292–4297.
47. Manosas M, Xi XG, Bensimon D, Croquette V (2010) Active and passive mechanisms of helicases. *Nucleic Acids Res* 38(16):5518–5526.
48. Carter BC, Vershinin M, Gross SP (2008) A comparison of step-detection methods: How well can you do? *Biophys J* 94(1):306–319.
49. Seol Y, Strub MP, Neuman KC (2016) Single molecule measurements of DNA helicase activity with magnetic tweezers and t-test based step-finding analysis. *Methods* 105: 119–127.
50. Johnson KA, Simpson ZB, Blom T (2009) Global kinetic explorer: A new computer program for dynamic simulation and fitting of kinetic data. *Anal Biochem* 387(1): 20–29.
51. Rad B, Forget AL, Baskin RJ, Kowalczykowski SC (2015) Single-molecule visualization of RecQ helicase reveals DNA melting, nucleation, and assembly are required for processive DNA unwinding. *Proc Natl Acad Sci USA* 112(50):E6852–E6861.
52. Wang ZX (1995) An exact mathematical expression for describing competitive binding of two different ligands to a protein molecule. *FEBS Lett* 360(2):111–114.
53. Young MC, Kuhl SB, von Hippel PH (1994) Kinetic theory of ATP-driven translocases on one-dimensional polymer lattices. *J Mol Biol* 235(5):1436–1446.
54. Rad B, Kowalczykowski SC (2012) Translocation of *E. coli* RecQ helicase on single-stranded DNA. *Biochemistry* 51(13):2921–2929.
55. Gyimesi M, Sarlós K, Derényi I, Kovács M (2010) Streamlined determination of processive run length and mechanochemical coupling of nucleic acid motor activities. *Nucleic Acids Res* 38(7):e102.
56. Hinz JM (2010) Role of homologous recombination in DNA interstrand crosslink repair. *Environ Mol Mutagen* 51(6):582–603.
57. Dillingham MS, Kowalczykowski SC (2008) RecBCD enzyme and the repair of double-stranded DNA breaks. *Microbiol Mol Biol Rev* 72(4):642–671.
58. Courcelle J (2005) Recs preventing wrecks. *Mutat Res* 577(1-2):217–227.
59. Nakayama H (2005) *Escherichia coli* RecQ helicase: A player in thymineless death. *Mutat Res* 577(1-2):228–236.
60. Sundin O, Varshavsky A (1981) Arrest of segregation leads to accumulation of highly intertwined catenated dimers: Dissection of the final stages of SV40 DNA replication. *Cell* 25(3):659–669.
61. Shereda RD, Reiter NJ, Butcher SE, Keck JL (2009) Identification of the SSB binding site on *E. coli* RecQ reveals a conserved surface for binding SSB's C terminus. *J Mol Biol* 386(3):612–625.
62. Shereda RD, Kozlov AG, Lohman TM, Cox MM, Keck JL (2008) SSB as an organizer/mobilizer of genome maintenance complexes. *Crit Rev Biochem Mol Biol* 43(5): 289–318.
63. Janscak P, et al. (2003) Characterization and mutational analysis of the RecQ core of the Bloom syndrome protein. *J Mol Biol* 330(1):29–42.